
Applied Superconductivity:

Josephson Effect and Superconducting Electronics

**Manuscript to the Lectures during WS 2003/2004, WS 2005/2006, WS 2006/2007,
WS 2007/2008, WS 2008/2009, and WS 2009/2010**

Prof. Dr. Rudolf Gross

and

Dr. Achim Marx

Walther-Meißner-Institut

Bayerische Akademie der Wissenschaften

and

Lehrstuhl für Technische Physik (E23)

Technische Universität München

Walther-Meißner-Strasse 8

D-85748 Garching

Rudolf.Gross@wmi.badw.de

Contents

Preface	xxi
I Foundations of the Josephson Effect	1
1 Macroscopic Quantum Phenomena	3
1.1 The Macroscopic Quantum Model	3
1.1.1 Coherent Phenomena in Superconductivity	3
1.1.2 Macroscopic Quantum Currents in Superconductors	12
1.1.3 The London Equations	18
1.2 Flux Quantization	24
1.2.1 Flux and Fluxoid Quantization	26
1.2.2 Experimental Proof of Flux Quantization	28
1.2.3 Additional Topic: Rotating Superconductor	30
1.3 Josephson Effect	32
1.3.1 The Josephson Equations	33
1.3.2 Josephson Tunneling	37
2 JJs: The Zero Voltage State	43
2.1 Basic Properties of Lumped Josephson Junctions	44
2.1.1 The Lumped Josephson Junction	44
2.1.2 The Josephson Coupling Energy	45
2.1.3 The Superconducting State	47
2.1.4 The Josephson Inductance	49
2.1.5 Mechanical Analogs	49
2.2 Short Josephson Junctions	50
2.2.1 Quantum Interference Effects – Short Josephson Junction in an Applied Magnetic Field	50

2.2.2	The Fraunhofer Diffraction Pattern	54
2.2.3	Determination of the Maximum Josephson Current Density	58
2.2.4	Additional Topic: Direct Imaging of the Supercurrent Distribution	62
2.2.5	Additional Topic: Short Josephson Junctions: Energy Considerations	63
2.2.6	The Motion of Josephson Vortices	65
2.3	Long Josephson Junctions	68
2.3.1	The Stationary Sine-Gordon Equation	68
2.3.2	The Josephson Vortex	70
2.3.3	Junction Types and Boundary Conditions	73
2.3.4	Additional Topic: Josephson Current Density Distribution and Maximum Josephson Current	79
2.3.5	The Pendulum Analog	84
3	JJs: The Voltage State	89
3.1	The Basic Equation of the Lumped Josephson Junction	90
3.1.1	The Normal Current: Junction Resistance	90
3.1.2	The Displacement Current: Junction Capacitance	92
3.1.3	Characteristic Times and Frequencies	93
3.1.4	The Fluctuation Current	94
3.1.5	The Basic Junction Equation	96
3.2	The Resistively and Capacitively Shunted Junction Model	97
3.2.1	Underdamped and Overdamped Josephson Junctions	100
3.3	Response to Driving Sources	102
3.3.1	Response to a dc Current Source	102
3.3.2	Response to a dc Voltage Source	107
3.3.3	Response to ac Driving Sources	107
3.3.4	Photon-Assisted Tunneling	112
3.4	Additional Topic: Effect of Thermal Fluctuations	115
3.4.1	Underdamped Junctions: Reduction of I_c by Premature Switching	117
3.4.2	Overdamped Junctions: The Ambegaokar-Halperin Theory	118
3.5	Secondary Quantum Macroscopic Effects	122
3.5.1	Quantum Consequences of the Small Junction Capacitance	122

3.5.2	Limiting Cases: The Phase and Charge Regime	125
3.5.3	Coulomb and Flux Blockade	128
3.5.4	Coherent Charge and Phase States	130
3.5.5	Quantum Fluctuations	132
3.5.6	Macroscopic Quantum Tunneling	133
3.6	Voltage State of Extended Josephson Junctions	139
3.6.1	Negligible Screening Effects	139
3.6.2	The Time Dependent Sine-Gordon Equation	140
3.6.3	Solutions of the Time Dependent Sine-Gordon Equation	141
3.6.4	Additional Topic: Resonance Phenomena	144
II	Applications of the Josephson Effect	153
4	SQUIDS	157
4.1	The dc-SQUID	159
4.1.1	The Zero Voltage State	159
4.1.2	The Voltage State	164
4.1.3	Operation and Performance of dc-SQUIDS	168
4.1.4	Practical dc-SQUIDS	172
4.1.5	Read-Out Schemes	176
4.2	Additional Topic: The rf-SQUID	180
4.2.1	The Zero Voltage State	180
4.2.2	Operation and Performance of rf-SQUIDS	182
4.2.3	Practical rf-SQUIDS	186
4.3	Additional Topic: Other SQUID Configurations	188
4.3.1	The DROS	188
4.3.2	The SQIF	189
4.3.3	Cartwheel SQUID	189
4.4	Instruments Based on SQUIDS	191
4.4.1	Magnetometers	192
4.4.2	Gradiometers	194
4.4.3	Susceptometers	196

4.4.4	Voltmeters	197
4.4.5	Radiofrequency Amplifiers	198
4.5	Applications of SQUIDs	200
4.5.1	Biomagnetism	200
4.5.2	Nondestructive Evaluation	204
4.5.3	SQUID Microscopy	206
4.5.4	Gravity Wave Antennas and Gravity Gradiometers	208
4.5.5	Geophysics	210
5	Digital Electronics	215
5.1	Superconductivity and Digital Electronics	216
5.1.1	Historical development	217
5.1.2	Advantages and Disadvantages of Josephson Switching Devices	219
5.2	Voltage State Josephson Logic	222
5.2.1	Operation Principle and Switching Times	222
5.2.2	Power Dissipation	225
5.2.3	Switching Dynamics, Global Clock and Punchthrough	226
5.2.4	Josephson Logic Gates	228
5.2.5	Memory Cells	234
5.2.6	Microprocessors	236
5.2.7	Problems of Josephson Logic Gates	237
5.3	RSFQ Logic	239
5.3.1	Basic Components of RSFQ Circuits	241
5.3.2	Information in RSFQ Circuits	246
5.3.3	Basic Logic Gates	247
5.3.4	Timing and Power Supply	249
5.3.5	Maximum Speed	249
5.3.6	Power Dissipation	250
5.3.7	Prospects of RSFQ	250
5.3.8	Fabrication Technology	253
5.3.9	RSFQ Roadmap	254
5.4	Analog-to-Digital Converters	255
5.4.1	Additional Topic: Foundations of ADCs	256
5.4.2	The Comparator	261
5.4.3	The Aperture Time	263
5.4.4	Different Types of ADCs	264

6	The Josephson Voltage Standard	269
6.1	Voltage Standards	270
6.1.1	Standard Cells and Electrical Standards	270
6.1.2	Quantum Standards for Electrical Units	271
6.2	The Josephson Voltage Standard	274
6.2.1	Underlying Physics	274
6.2.2	Development of the Josephson Voltage Standard	274
6.2.3	Junction and Circuit Parameters for Series Arrays	279
6.3	Programmable Josephson Voltage Standard	281
6.3.1	Pulse Driven Josephson Arrays	283
7	Superconducting Photon and Particle Detectors	285
7.1	Superconducting Microwave Detectors: Heterodyne Receivers	286
7.1.1	Noise Equivalent Power and Noise Temperature	286
7.1.2	Operation Principle of Mixers	287
7.1.3	Noise Temperature of Heterodyne Receivers	290
7.1.4	SIS Quasiparticle Mixers	292
7.1.5	Josephson Mixers	296
7.2	Superconducting Microwave Detectors: Direct Detectors	297
7.2.1	NEP of Direct Detectors	298
7.3	Thermal Detectors	300
7.3.1	Principle of Thermal Detection	300
7.3.2	Bolometers	302
7.3.3	Antenna-Coupled Microbolometers	307
7.4	Superconducting Particle and Single Photon Detectors	314
7.4.1	Thermal Photon and Particle Detectors: Microcalorimeters	314
7.4.2	Superconducting Tunnel Junction Photon and Particle Detectors	318
7.5	Other Detectors	328
8	Microwave Applications	329
8.1	High Frequency Properties of Superconductors	330
8.1.1	The Two-Fluid Model	330
8.1.2	The Surface Impedance	333
8.2	Superconducting Resonators and Filters	336
8.3	Superconducting Microwave Sources	337

9 Superconducting Quantum Bits	339
9.1 Quantum Bits and Quantum Computers	341
9.1.1 Quantum Bits	341
9.1.2 Quantum Computing	343
9.1.3 Quantum Error Correction	346
9.1.4 What are the Problems?	348
9.2 Implementation of Quantum Bits	349
9.3 Why Superconducting Qubits	352
9.3.1 Superconducting Island with Leads	352
III Anhang	355
A The Josephson Equations	357
B Imaging of the Maximum Josephson Current Density	361
C Numerical Iteration Method for the Calculation of the Josephson Current Distribution	363
D Photon Noise	365
I Power of Blackbody Radiation	365
II Noise Equivalent Power	367
E Qubits	369
I What is a quantum bit ?	369
I.1 Single-Qubit Systems	369
I.2 The spin-1/2 system	371
I.3 Two-Qubit Systems	372
II Entanglement	373
III Qubit Operations	375
III.1 Unitarity	375
III.2 Single Qubit Operations	375
III.3 Two Qubit Operations	376
IV Quantum Logic Gates	377
IV.1 Single-Bit Gates	377
IV.2 Two Bit Gates	379
V The No-Cloning Theorem	384
VI Quantum Complexity	385
VII The Density Matrix Representation	385

F	Two-Level Systems	389
I	Introduction to the Problem	389
I.1	Relation to Spin-1/2 Systems	390
II	Static Properties of Two-Level Systems	390
II.1	Eigenstates and Eigenvalues	390
II.2	Interpretation	391
II.3	Quantum Resonance	394
III	Dynamic Properties of Two-Level Systems	395
III.1	Time Evolution of the State Vector	395
III.2	The Rabi Formula	395
G	The Spin 1/2 System	399
I	Experimental Demonstration of Angular Momentum Quantization	399
II	Theoretical Description	401
II.1	The Spin Space	401
III	Evolution of a Spin 1/2 Particle in a Homogeneous Magnetic Field	402
IV	Spin 1/2 Particle in a Rotating Magnetic Field	404
IV.1	Classical Treatment	404
IV.2	Quantum Mechanical Treatment	406
IV.3	Rabi's Formula	407
H	Literature	409
I	Foundations of Superconductivity	409
I.1	Introduction to Superconductivity	409
I.2	Early Work on Superconductivity and Superfluidity	410
I.3	History of Superconductivity	410
I.4	Weak Superconductivity, Josephson Effect, Flux Structures	410
II	Applications of Superconductivity	411
II.1	Electronics, Sensors, Microwave Devices	411
II.2	Power Applications, Magnets, Transportation	412
II.3	Superconducting Materials	412
I	SI-Einheiten	413
I	Geschichte des SI Systems	413
II	Die SI Basiseinheiten	415
III	Einige von den SI Einheiten abgeleitete Einheiten	416
IV	Vorsätze	418
V	Abgeleitete Einheiten und Umrechnungsfaktoren	419

J Physikalische Konstanten**425**

List of Figures

1.1	Meissner-Effect	19
1.2	Current transport and decay of a supercurrent in the Fermi sphere picture	20
1.3	Stationary Quantum States	24
1.4	Flux Quantization in Superconductors	25
1.5	Flux Quantization in a Superconducting Cylinder	27
1.6	Experiment by Doll and Naebauer	29
1.7	Experimental Proof of Flux Quantization	29
1.8	Rotating superconducting cylinder	31
1.9	The Josephson Effect in weakly coupled superconductors	32
1.10	Variation of n_s^* and γ across a Josephson junction	35
1.11	Schematic View of a Josephson Junction	36
1.12	Josephson Tunneling	39
2.1	Lumped Josephson Junction	45
2.2	Coupling Energy and Josephson Current	46
2.3	The Tilted Washboard Potential	48
2.4	Extended Josephson Junction	51
2.5	Magnetic Field Dependence of the Maximum Josephson Current	55
2.6	Josephson Current Distribution in a Small Josephson Junction for Various Applied Magnetic Fields	56
2.7	Spatial Interference of Macroscopic Wave Funktionen	57
2.8	The Josephson Vortex	57
2.9	Gaussian Shaped Josephson Junction	59
2.10	Comparison between Measurement of Maximum Josephson Current and Optical Diffraction Experiment	60
2.11	Supercurrent Auto-correlation Function	61
2.12	Magnetic Field Dependence of the Maximum Josephson Current of a YBCO-GBJ	63

2.13	Motion of Josephson Vortices	66
2.14	Magnetic Flux and Current Density Distribution for a Josephson Vortex	70
2.15	Classification of Junction Types: Overlap, Inline and Grain Boundary Junction	74
2.16	Geometry of the Asymmetric Inline Junction	77
2.17	Geometry of Mixed Overlap and Inline Junctions	78
2.18	The Josephson Current Distribution of a Long Inline Junction	80
2.19	The Maximum Josephson Current as a Function of the Junction Length	81
2.20	Magnetic Field Dependence of the Maximum Josephson Current and the Josephson Current Density Distribution in an Overlap Junction	83
2.21	The Maximum Josephson Current as a Function of the Applied Field for Overlap and Inline Junctions	84
3.1	Current-Voltage Characteristic of a Josephson tunnel junction	91
3.2	Equivalent circuit for a Josephson junction including the normal, displacement and fluctuation current	92
3.3	Equivalent circuit of the Resistively Shunted Junction Model	97
3.4	The Motion of a Particle in the Tilt Washboard Potential	98
3.5	Pendulum analogue of a Josephson junction	99
3.6	The IVCs for Underdamped and Overdamped Josephson Junctions	101
3.7	The time variation of the junction voltage and the Josephson current	103
3.8	The RSJ model current-voltage characteristics	105
3.9	The RCSJ Model IVC at Intermediate Damping	107
3.10	The RCJ Model Circuit for an Applied dc and ac Voltage Source	108
3.11	Overdamped Josephson Junction driven by a dc and ac Voltage Source	110
3.12	Overdamped Josephson junction driven by a dc and ac Current Source	111
3.13	Shapiro steps for under- and overdamped Josephson junction	112
3.14	Photon assisted tunneling	113
3.15	Photon assisted tunneling in SIS Josephson junction	113
3.16	Thermally Activated Phase Slippage	116
3.17	Temperature Dependence of the Thermally Activated Junction Resistance	119
3.18	RSJ Model Current-Voltage Characteristics Including Thermally Activated Phase Slippage	120
3.19	Variation of the Josephson Coupling Energy and the Charging Energy with the Junction Area	124
3.20	Energy diagrams of an isolated Josephson junction	127
3.21	The Coulomb Blockade	128

3.22	The Phase Blockade	129
3.23	The Cooper pair box	131
3.24	Double well potential for the generation of phase superposition states	132
3.25	Macroscopic Quantum Tunneling	134
3.26	Macroscopic Quantum Tunneling at Large Damping	138
3.27	Mechanical analogue for phase dynamics of a long Josephson junction	141
3.28	The Current Voltage Characteristic of an Underdamped Long Josephson Junction	145
3.29	Zero field steps in IVCs of an annular Josephson junction	147
4.1	The dc-SQUID	160
4.2	Maximum Supercurrent versus Applied Magnetic Flux for a dc-SQUID at Weak Screening	162
4.3	Total Flux versus Applied Magnetic Flux for a dc SQUID at $\beta_L > 1$	163
4.4	Current-voltage Characteristics of a dc-SQUID at Negligible Screening	165
4.5	The pendulum analogue of a dc SQUID	167
4.6	Principle of Operation of a dc-SQUID	169
4.7	Energy Resolution of dc-SQUIDs	172
4.8	The Practical dc-SQUID	173
4.9	Geometries for thin film SQUID washers	174
4.10	Flux focusing effect in a $\text{YBa}_2\text{Cu}_3\text{O}_{7-\delta}$ washer	175
4.11	The Washer dc-SQUID	176
4.12	The Flux Modulation Scheme for a dc-SQUID	177
4.13	The Modulation and Feedback Circuit of a dc-SQUID	178
4.14	The rf-SQUID	180
4.15	Total flux versus applied flux for a rf-SQUID	182
4.16	Operation of rf-SQUIDs	183
4.17	Tank voltage versus rf-current for a rf-SQUID	184
4.18	High T_c rf-SQUID	187
4.19	The double relaxation oscillation SQUID (DROS)	188
4.20	The Superconducting Quantum Interference Filter (SQIF)	190
4.21	Input Antenna for SQUIDs	191
4.22	Various types of thin film SQUID magnetometers	193
4.23	Magnetic noise signals	194
4.24	Magnetically shielded room	195
4.25	Various gradiometers configurations	196

4.26	Miniature SQUID Susceptometer	197
4.27	SQUID Radio-frequency Amplifier	198
4.28	Multichannel SQUID Systems	201
4.29	Magnetocardiography	203
4.30	Magnetic field distribution during R peak	204
4.31	SQUID based nondestructive evaluation	205
4.32	Scanning SQUID microscopy	207
4.33	Scanning SQUID microscopy images	208
4.34	Gravity wave antenna	209
4.35	Gravity gradiometer	210
5.1	Cryotron	217
5.2	Josephson Cryotron	218
5.3	Device performance of Josephson devices	220
5.4	Principle of operation of a Josephson switching device	222
5.5	Output current of a Josephson switching device	224
5.6	Threshold characteristics for a magnetically and directly coupled gate	229
5.7	Three-junction interferometer gate	230
5.8	Current injection device	230
5.9	Josephson Atto Weber Switch (JAWS)	231
5.10	Direct coupled logic (DCL) gate	231
5.11	Resistor coupled logic (RCL) gate	232
5.12	4 junction logic (4JL) gate	232
5.13	Non-destructive readout memory cell	234
5.14	Destructive read-out memory cell	235
5.15	4 bit Josephson microprocessor	237
5.16	Josephson microprocessor	238
5.17	Comparison of latching and non-latching Josephson logic	240
5.18	Generation of SFQ Pulses	242
5.19	dc to SFQ Converter	243
5.20	Basic Elements of RSFQ Circuits	244
5.21	RSFQ memory cell	245
5.22	RSFQ logic	246
5.23	RSFQ OR and AND Gate	247

5.24	RSFQ NOT Gate	248
5.25	RSFQ Shift Register	249
5.26	RSFQ Microprocessor	253
5.27	RSFQ roadmap	254
5.28	Principle of operation of an analog-to-digital converter	256
5.29	Analog-to-Digital Conversion	257
5.30	Semiconductor and Superconductor Comparators	262
5.31	Incremental Quantizer	263
5.32	Flash-type ADC	265
5.33	Counting-type ADC	266
6.1	Weston cell	271
6.2	The metrological triangle for the electrical units	273
6.3	IVC of an underdamped Josephson junction under microwave irradiation	275
6.4	International voltage comparison between 1920 and 2000	276
6.5	One-Volt Josephson junction array	277
6.6	Josephson series array embedded into microwave stripline	278
6.7	Microwave design of Josephson voltage standards	279
6.8	Adjustment of Shapiro steps for a series array Josephson voltage standard	281
6.9	IVC of overdamped Josephson junction with microwave irradiation	282
6.10	Programmable Josephson voltage standard	283
7.1	Block diagram of a heterodyne receiver	288
7.2	Ideal mixer as a switch	288
7.3	Current response of a heterodyne mixer	289
7.4	IVCs and IF output power of SIS mixer	290
7.5	Optimum noise temperature of a SIS quasiparticle mixer	293
7.6	Measured DSB noise temperature of a SIS quasiparticle mixers	294
7.7	High frequency coupling schemes for SIS mixers	295
7.8	Principle of thermal detectors	301
7.9	Operation principle of superconducting transition edge bolometer	302
7.10	Sketch of a HTS bolometer	305
7.11	Specific detectivity of various bolometers	305
7.12	Relaxation processes in a superconductor after energy absorption	307
7.13	Antenna-coupled microbolometer	308

7.14	Schematic illustration of the hot electron bolometer mixer	309
7.15	Hot electron bolometer mixers with different antenna structures	311
7.16	Transition-edge sensors	315
7.17	Transition-edge sensors	317
7.18	Functional principle of a superconducting tunnel junction detector	319
7.19	Circuit diagram of a superconducting tunnel junction detector	319
7.20	Energy resolving power of STJDs	321
7.21	Quasiparticle tunneling in SIS junctions	323
7.22	Quasiparticle trapping in STJDs	326
7.23	STJDs employing lateral quasiparticle trapping	326
7.24	Superconducting tunnel junction x-ray detector	327
8.1	Equivalent circuit for the two-fluid model	332
8.2	Characteristic frequency regimes for a superconductor	332
8.3	Surface resistance of Nb and Cu	335
9.1	Konrad Zuse 1945	341
9.2	Representation of a Qubit State as a Vector on the Bloch Sphere	342
9.3	Operational Scheme of a Quantum Computer	344
9.4	Quantum Computing: What's it good for?	345
9.5	Shor, Feynman, Bennett and Deutsch	346
9.6	Qubit Realization by Quantum Mechanical Two level System	349
9.7	Use of Superconductors for Qubits	352
9.8	Superconducting Island with Leads	354
E.1	The Bloch Sphere S^2	370
E.2	The Spin-1/2 System	371
E.3	Entanglement – an artist's view.	373
E.4	Classical Single-Bit Gate	377
E.5	Quantum NOT Gate	378
E.6	Classical Two Bit Gate	380
E.7	Reversible and Irreversible Logic	380
E.8	Reversible Classical Logic	381
E.9	Reversible XOR (CNOT) and SWAP Gate	382
E.10	The Controlled U Gate	382

E.11	Density Matrix for Pure Single Qubit States	386
E.12	Density Matrix for a Coherent Superposition of Single Qubit States	387
F.1	Energy Levels of a Two-Level System	392
F.2	The Benzene Molecule	394
F.3	Graphical Representation of the Rabi Formula	396
G.1	The Larmor Precession	400
G.2	The Rotating Reference Frame	404
G.3	The Effective Magnetic Field in the Rotating Reference Frame	405
G.4	Rabi's Formula for a Spin 1/2 System	408

List of Tables

5.1	Switching delay and power dissipation for various types of logic gates.	233
5.2	Josephson 4 kbit RAM characteristics (organization: 4096 word × 1 bit, NEC).	236
5.3	Performance of various logic gates	237
5.4	Possible applications of superconductor digital circuits (source: SCENET 2001).	251
5.5	Performance of various RSFQ based circuits.	252
7.1	Characteristic materials properties of some superconductors	325
8.1	Important high-frequency characteristic of superconducting and normal conducting . . .	334
E.1	Successive measurements on a two-qubit state showing the results A and B with the corresponding probabilities $P(A)$ and $P(B)$ and the remaining state after the measurement. . . .	373

Chapter 8

Microwave Applications

Superconducting devices find brought applications in passive microwave devices such as filters or resonators. These applications are based on the very small losses due to the small microwave surface resistance of superconducting materials. Therefore, the quality factor of superconducting microwave resonators and filters is larger than for equally sized normalconducting devices. In the same way, at the same quality factor superconducting microwave resonators and filters can be made much smaller. This is in particular important for satellite or space applications. In this Chapter we briefly discuss the foundations of superconducting passive microwave devices and describe a few prominent devices structures and applications.

Superconducting devices based on Josephson junctions can serve as sources for microwave radiation. Here, the underlying principle is based on the voltage-frequency relation $V = f\Phi_0$, which immediately suggests that a Josephson junction can be used as a voltage controlled oscillator with $f/V = 483\,597.9$ GHz/V. In this Chapter we also present the foundations of superconducting microwave sources based on Josephson junction.

8.1 High Frequency Properties of Superconductors

8.1.1 The Two-Fluid Model

Already in 1934, that is long before the development of BCS theory, **Cornelius Gorter** and **H.B.G. Casimir** developed the two fluid model of superconductors.^{1,2} The model is based on the concept that there are two fluids in superconductors, namely a superfluid with carrier density n_s and a normal fluid with carrier density n_n with the total carrier density given by

$$n = n_n + \frac{n_s}{2} . \quad (8.1.1)$$

Here, the factor $\frac{1}{2}$ arises from the fact that the carriers of the superfluid are pairs with charge $-2e$. We will use the two-fluid model together with Ohm's law

$$\frac{1}{\sigma_n} \mathbf{J}_n = \mathbf{E} \quad (8.1.2)$$

and the linearized first London equation (compare (1.1.70) and (1.1.71))

$$\frac{\partial}{\partial t}(\Lambda \mathbf{J}_s) = \frac{\partial}{\partial t}(\mu_0 \lambda_L^2 \mathbf{J}_s) = \mathbf{E} \quad (8.1.3)$$

to describe the relation of the normal and superfluid current density and the electric field. In (8.1.3)

$$\Lambda \equiv \frac{m_s^*}{n_s^* q^{*2}} \quad (8.1.4)$$

is the *London coefficient* and

$$\lambda_L \equiv \sqrt{\frac{m_s^*}{\mu_0 n_s^* q^{*2}}} \quad (8.1.5)$$

the *London penetration depth* (compare (1.1.63) and (1.1.64)). Here, $q^* = -2e$ and m_s^* are the charge and the effective mass of the carrier forming the superfluid.

For a harmonic current with angular frequency ω (8.1.3) can be written as

$$i\omega \Lambda \mathbf{J}_s = i\omega \mu_0 \lambda_L^2 \mathbf{J}_s = \frac{1}{\sigma_s} \mathbf{J}_s = \mathbf{E} \quad (8.1.6)$$

with the purely imaginary conductivity of the superfluid

$$\sigma_s = \frac{n_s^* q^{*2}}{i\omega m_s^*} = \frac{1}{i\omega \Lambda} = \frac{1}{i\omega \mu_0 \lambda_L^2} . \quad (8.1.7)$$

¹D. Shoenberg, *Superconductivity*, Cambridge University Press, Cambridge (1965), pp. 194-196.

²T. van Duzer, *Principles of Superconducting Devices and Circuits*, Elsevier, New York, Amsterdam, London (1981), p. 124.

To derive the equivalent relations for the normal fluid we write the normal current as $\mathbf{J}_n = n_n e \mathbf{v}_n$, where \mathbf{v}_n is the average velocity of the normal carriers, and assume that the normal carriers have to satisfy Newton's law³

$$m_n^* \left(\frac{d\mathbf{v}_n}{dt} + \frac{\mathbf{v}_n}{\tau} \right) = e\mathbf{E} . \quad (8.1.8)$$

Here, τ is the scattering time of the normal carriers and m_n^* and e the effective mass and charge of the normal carriers. Again, for a sinusoidal current with angular frequency ω we obtain

$$\mathbf{J}_n = \left(\frac{n_n e^2}{m_n^*} \right) \frac{\tau}{1 + i\omega\tau} \mathbf{E} = \sigma_n \mathbf{E} . \quad (8.1.9)$$

The complex conductivity of the normal current can be expressed as

$$\sigma_n = \sigma_{n1} - i\sigma_{n2} = \left(\frac{n_n e^2 \tau}{m_n^*} \right) \frac{1 - i\omega\tau}{1 + (\omega\tau)^2} = \sigma_0 \frac{n_n}{n} \frac{1 - i\omega\tau}{1 + (\omega\tau)^2} . \quad (8.1.10)$$

Here, $\sigma_0 = n_n e^2 \tau / m_n^*$ is the usual normal state Drude conductivity. With (8.1.2), (8.1.3) and (8.1.6) together with the expressions for the conductivities and Maxwell's equations we can derive the high-frequency properties of superconductors.

Note that the conductivities σ_n and σ_s show a strong temperature dependence below T_c due to the temperature variation of the normal and superfluid density. At $T = T_c$ we have $n_s = 0$ and $n_n = n$. Below T_c the superfluid density increases and the normal fluid density decreases as

$$\frac{n_n}{n} = \left(\frac{T}{T_c} \right)^4 \quad (8.1.11)$$

$$\frac{n_s}{2n} = 1 - \left(\frac{T}{T_c} \right)^4 . \quad (8.1.12)$$

At $T = 0$ all the carriers are condensed into the superfluid and we have $n_s = n/2$ and $n_n = 0$.

In an electrotechnical language the two-fluid model can be visualized by the equivalent circuit shown in Fig. 8.1. The superfluid channel which does not contribute to the loss and has purely imaginary conductivity can be modeled by an inductor $L_s(T)$. The normal channel has a conductivity composed of a imaginary and a real part. The former, represented by the inductor $L_n(T)$, is due to the inertia of the charge carriers and the latter, represented by the resistor $R_n(T)$, due scattering induced loss. Note that the inductor L_n in the normal channel is often neglected which is similar to modeling the normal channel as nondispersive (frequency independent).

We can use the equivalent circuit to classify different frequency regimes. Evidently at $\omega = 0$ all the current is carried by the nondissipative superconducting channel. However, increasing the frequency the conductivity of the superfluid density becomes finite and decreases with frequency. Therefore, the contribution of \mathbf{J}_s decreases with increasing frequency and becomes equal to \mathbf{J}_n at the cross-over frequency $\omega_{ns} = R_n/L_s$. That is, the superfluid dominates in the low-frequency regime $0 \leq \omega \leq \omega_{ns}$. In the high-frequency regime the normal channel dominates. We further can discuss the question at which frequency there is a cross-over between an ohmic (nondispersive) response to an inductive (dispersive) response in

³The quantity e represents the unit of the electric charge with an electron having the charge $-e$.

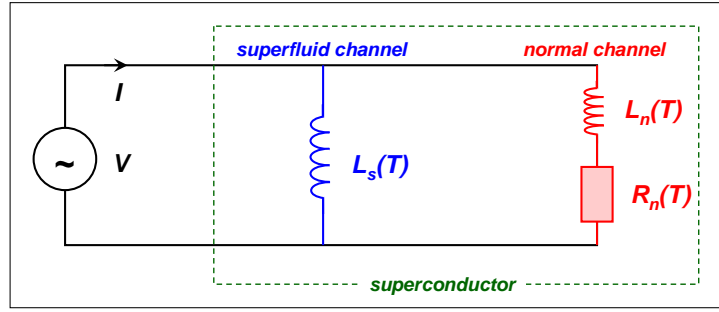


Figure 8.1: Equivalent circuit for the two-fluid model of a superconductor.

the normal channel. Evidently this occurs at the frequency $\omega_\tau = R_n/L_n = 1/\tau$. That is, in the frequency regime $\omega_{ns} \leq \omega \leq 1/\tau$ the ohmic response and for $\omega \geq 1/\tau$ the inductive response of the normal channel is dominant. In the high-frequency regime we restrict our discussion to $\omega < \omega_\Delta = \Delta/\hbar$. Above the gap frequency ω_Δ the microwave photons can break up Cooper pairs and the situation becomes more complicated. For a superconductor with $\Delta = 1$ meV the gap frequency ω_Δ is about 1 THz. Note that $\tau_{ns} = L_s/R_n$ increases strongly with decreasing temperature due to the increase of L_s and the decrease of R_n associated with the temperature variation of n_n and n_s . Therefore, the cross-over frequency ω_{ns} increase with decreasing temperature and typically becomes larger than ω_τ as shown in Fig. 8.2. In this case there is no frequency regime where the ohmic normal channel dominates.

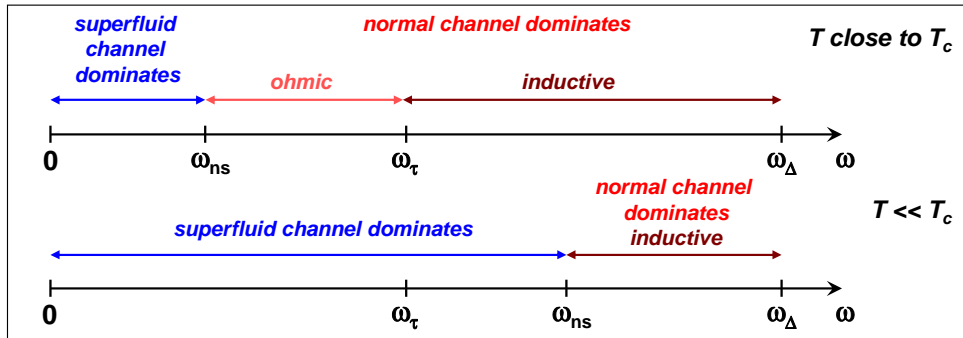


Figure 8.2: Characteristic frequency regimes for a superconductor for different temperatures.

Using equations (8.1.7) and (8.1.10) we obtain the total conductivity of a superconductor to

$$\sigma = \sigma_s + \sigma_n = \frac{n_n e^2 \tau}{m_n^*} \frac{1}{1 + (\omega\tau)^2} - i \frac{n_n e^2 \tau}{m_n^*} \frac{\omega\tau}{1 + (\omega\tau)^2} - i \frac{1}{\omega \mu_0 \lambda_L^2} \quad (8.1.13)$$

At frequencies $\omega\tau \ll 1$ this can be simplified to

$$\sigma = \sigma_1 - i\sigma_2 = \frac{n_n e^2 \tau}{m_n^*} - i \frac{1}{\omega \mu_0 \lambda_L^2}, \quad (8.1.14)$$

where σ_1 and σ_2 are the real and imaginary components of the complex conductivity. The real part represents the loss from the normal carriers, whereas the imaginary part represents the kinetic energy of the superconductive carriers.

8.1.2 The Surface Impedance

Normal Metals

The surface impedance is defined as the characteristic impedance seen by a plane wave incident perpendicular upon a flat surface of a conductor. It is given by the ratio of the electric and the magnetic field at the surface. For thick normalconducting materials the surface impedance is equal to the bulk wave impedance Z which can be derived from Maxwell's equations to

$$Z_s = R_s + iX_s = \sqrt{\frac{i\mu_0\omega}{\sigma_0}} = (1+i)\sqrt{\frac{\mu_0\omega}{2\sigma_0}} = (1+i)\frac{\mu_0\omega\delta_0}{2}. \quad (8.1.15)$$

Here, $\sigma_0 = ne^2\tau/m^*$ is the normal state conductivity and

$$\delta_0 = \sqrt{\frac{2}{\mu_0\omega\sigma_0}} \quad (8.1.16)$$

is the normal state field penetration depth. For a normal metal at frequencies $\omega\tau \ll 1$, i.e. in the ohmic regime, the conductivity is a real number and according to (8.1.16) the surface resistance R_s and the surface reactance X_s are equal:

$$R_s = X_s = \sqrt{\frac{\mu_0\omega}{2\sigma_0}} = \frac{\mu_0\omega\delta_0}{2}. \quad (8.1.17)$$

We see that for normal metals both R_s and X_s are proportional to $\sqrt{\omega}$.

Superconductors

In order to derive the surface impedance of a superconductor we the normal state conductivity σ_0 in (8.1.16) by the total conductivity of a superconductor and obtain

$$\begin{aligned} Z_s = R_s + iX_s &= \sqrt{\frac{i\mu_0\omega}{\sigma}} = \left[\frac{\sigma_n \frac{1}{1+(\omega\tau)^2} - i\sigma_n \frac{\omega\tau}{1+(\omega\tau)^2} - i\frac{1}{\omega\mu_0\lambda_L^2}}{i\omega\mu_0} \right]^{-1/2} \\ &= i\omega\mu_0 \left[i\omega\mu_0\sigma_n \frac{1}{1+(\omega\tau)^2} + \omega\mu_0\sigma_n \frac{\omega\tau}{1+(\omega\tau)^2} + \frac{1}{\lambda_L^2} \right]^{-1/2}. \end{aligned} \quad (8.1.18)$$

At frequencies $\omega\tau \ll 1$ this can be simplified to

$$Z_s = \frac{i\omega\mu_0}{\lambda_L} [1 + i\omega\mu_0\lambda_L^2\sigma_n]^{-1/2} = i\sqrt{\frac{\omega\mu_0}{\sigma_2}} \left[1 + i\frac{\sigma_1}{\sigma_2} \right]^{-1/2}, \quad (8.1.19)$$

where we have used $\sigma = \sigma_1 + i\sigma_2$ with $\sigma_1 = \sigma_n$ and $\sigma_2 = 1/\omega\mu_0\lambda_L^2$. We can now further simplify (8.1.19) by taking into account that $\sigma_1 \ll \sigma_2$ for temperatures not too close to T_c . With $(1+x)^{-1/2} \simeq 1 - \frac{1}{2}x$ we obtain

$$Z_s = i\sqrt{\frac{\omega\mu_0}{\sigma_2}} \left(1 - i\frac{\sigma_1}{2\sigma_2} \right) = \sqrt{\frac{\omega\mu_0\sigma_1^2}{2\sigma_2^3}} + i\sqrt{\frac{\omega\mu_0}{\sigma_2}}. \quad (8.1.20)$$

Table 8.1: Conductivity σ , penetration depth δ_0 due to the normal skin effect, London penetration depth λ_L , surface resistance R_s and surface reactance X_s of normal conductors and superconductors for $\omega\tau \ll 1$ and temperatures $T \ll T_c$.

	normal conductor	superconductor
conductivity	$\sigma_0 = \frac{ne^2\tau}{m_n^*}$	$\sigma_1 + i\sigma_2 = \frac{ne^2\tau}{m_n^*} \left(\frac{n_n}{n}\right) - i\frac{1}{\omega\mu_0\lambda_L^2}$
field penetration depth	$\delta_0 = \sqrt{2/\omega\mu_0\sigma_0}$	$\delta_s = \lambda_L$
surface resistance	$R_s = \frac{1}{2}\omega\mu_0\delta_0 = \sqrt{\frac{\omega\mu_0}{2\sigma_0}}$	$R_s = \frac{1}{2}\omega^2\mu_0^2\lambda_L^3\sigma_0 \left(\frac{n_n}{n}\right)$
surface reactance	$X_s = \frac{1}{2}\omega\mu_0\delta_0 = \sqrt{\frac{\omega\mu_0}{2\sigma_0}}$	$X_s = \omega\mu_0\lambda_L$

Using expression (8.1.14) for σ_1 and σ_2 we finally obtain

$$Z_s = R_s + iX_s = \frac{\omega^2\mu_0^2\lambda_L^3n_n e^2\tau}{2m_n^*} + i\omega\mu_0\lambda_L = \frac{1}{2}\omega^2\mu_0^2\lambda_L^3\sigma_0 \left(\frac{n_n}{n}\right) + i\omega\mu_0\lambda_L. \quad (8.1.21)$$

We see that the surface resistance, the real part of Z_s , increases proportional to ω^2 in contrast to normal conductors, where $R_s \propto \sqrt{\omega}$. Furthermore, it increases proportional to λ_L^3 and the conductivity $\sigma_0 n_n/n$ of the normal fluid. In Table 8.1 the most main characteristics of superconductors are compared to those of normal metals.

Fig. 8.3 shows the theoretically expected surface resistance as a function of frequency for the superconductor Nb and the normal metal Cu. We see that for frequencies below about 100 GHz the surface resistance of Nb is considerably lower than for Cu at 77 K. At high frequencies there is a cross-over due to the much weaker frequency dependence of the surface resistance of normal metals. Note that the surface resistance is expected to be further reduced by going to lower temperatures due to the strong decrease of n_n . At $T/T_c \ll 1$, $\lambda_L(T) \simeq \text{const}$ and $n_n \propto \exp(-2\Delta_0/k_B T)$. Therefore, an exponential decrease of R_s with decreasing T is expected. However, this behavior is usually not observed in experiment. Rather a temperature independent residual surface resistance is measured at very low T , which is attributed to material defects. For Nb this residual resistance is as low as $10^{-9}\Omega/\square$ at 10 GHz, whereas it reaches only about $10^{-5}\Omega/\square$ for $\text{YBa}_2\text{Cu}_3\text{O}_{7-\delta}$ films.

Kinetic Inductance

The surface reactance X_s , the imaginary part of the surface impedance, is purely inductive. The equivalent inductance L_k is denoted as *kinetic inductance*

$$L_k = \mu_0\lambda_L. \quad (8.1.22)$$

The kinetic inductance reflects the kinetic energy of the carriers of the superfluid.

Finally we note that the phenomenological model used above is based on local theory, which is valid only as long as the coherence length ξ of a superconductor is much smaller than the London penetration

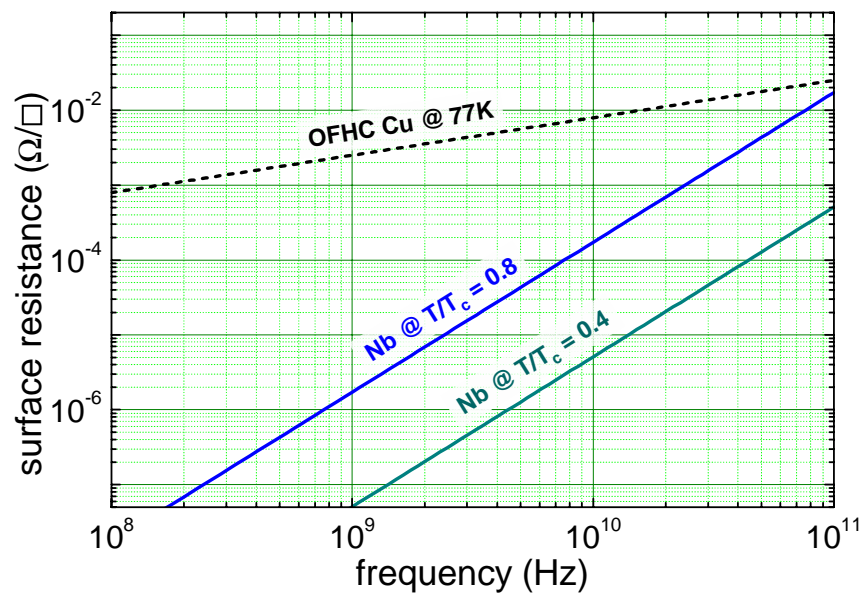


Figure 8.3: Intrinsic surface resistance versus frequency for Nb and oxygen free high conductance (OFHC) Cu. For Cu, $\sigma_0 = 10^8 \Omega^{-1} \text{m}^{-1}$, for Nb, $\lambda(0) = 85 \text{ nm}$ and $\sigma_0 = 10^8 \Omega^{-1} \text{m}^{-1}$ were used.

depth λ_L . This is for example the case for extreme type-II superconductors such as the high temperature superconductors. In contrast, for type-I superconductors we have $\xi > \lambda_L$. In this case the above treatment is non longer valid and we have to used a more complicated nonlocal theory.⁴

⁴A.B. Pippard, *An experimental and theoretical study of the relation between magnetic field and current in a superconductor*, Proc. Roy. Soc. (London), A **216**, 547-568 (1963).

8.2 Superconducting Resonators and Filters

in preparation

8.3 Superconducting Microwave Sources

in preparation